MOLECULAR CHEMISTRY

10.1126/sciadv.1600579

Reorganization of hydrogen bond network makes strong polyelectrolyte brushes pH-responsive

Bo Wu,[1,2] Xiaowen Wang,[1] Jun Yang,[1] Zan Hua,[1] Kangzhen Tian,[1] Ran Kou,[1] Jian Zhang,[1] Shuji Ye,[1]* Yi Luo,[1]* Vincent S. J. Craig,[3] Guangzhao Zhang,[2]* Guangming Liu[1]*

Weak polyelectrolytes have found extensive practical applications owing to their rich pH-responsive properties. In contrast, strong polyelectrolytes have long been regarded as pH-insensitive based on the well-established fact that the average degree of charging of strong polyelectrolyte chains is independent of pH. The possible applications of strong polyelectrolytes in smart materials have, thus, been severely limited. However, we demonstrate that almost all important properties of strong polyelectrolyte brushes (SPBs), such as chain conformation, hydration, stiffness, surface wettability, lubricity, adhesion, and protein adsorption are sensitive to pH. The pH response originates from the reorganization of the interchain hydrogen bond network between the grafted chains, triggered by the pH-mediated adsorption-desorption equilibrium of hydronium or hydroxide with the brushes. The reorganization process is firmly identified by advanced sum-frequency generation vibrational spectroscopy. Our findings not only provide a new understanding of the fundamental properties of SPBs but also uncover an extensive family of building blocks for constructing pH-responsive materials.

INTRODUCTION

Strong polyelectrolytes (SPs), representing a large group of polymeric materials, have been found to have many important applications in the fields of energy, environment, and health (*1*–*3*). However, they are not used in circumstances in which pH response is required because of the widely held view that they are insensitive to pH changes (*4*–*7*). This view is based on the insensitivity of the polymer charge of SPs to variations in pH (*8*, *9*). This has prevented SPs from being used in applications, such as energy storage devices (*1*), water treatment (*2*), and catalysis (*10*), when it is required that either the mechanical strength of electrolyte, the antifouling properties of membranes, or the efficiency of immobilized catalyst, respectively, are pH-dependent. Here, we use SP brushes (SPBs) as a well-controlled model system to systematically examine the pH-responsive properties of SPs and find that SPBs are pH-dependent because of the pH dependence of interchain hydrogen bonding interactions. The demonstrated pH response indicates that SPs will be found to have wide applications as pH-responsive agents, for which it is important that the electrostatic interaction remains constant during the modulation of pH, such as in drug delivery (*6*), tribology (*11*, *12*), and emulsification (*13*) applications.

RESULTS

Macroscopic pH-responsive properties of positively charged SPBs

We first demonstrate that the macroscopic properties of SPBs are dependent on pH, using several different experimental techniques. Positively charged poly[2-(methacryloyloxy)ethyl trimethylammonium chloride] (PMETAC) and negatively charged poly(3-sulfopropyl methacrylate potassium) (PSPMA) brushes were prepared with the surface-initiated atom transfer radical polymerization (SI-ATRP) method to demonstrate the pH-responsive nature of SPBs. To discount the influence of ionic strength, constant–ionic strength solutions (that is, 10 mM) with different pH values were prepared using HCl, KCl, and KOH. A quartz crystal microbalance with dissipation (QCM-D) was used to measure the shifts in frequency (Δf) and dissipation (ΔD) of SPBs with pH. According to the Sauerbrey equation, the increase in Δf of the PMETAC brushes in Fig. 1A indicates that the mass associated with the cationic SPBs decreases (that is, dehydration) with increasing pH and vice versa (*14*, *15*). The associated decrease in ΔD indicates that the cationic SPBs become stiffer with increasing pH and vice versa. The time scale for the pH-responsive behavior of the PMETAC brushes in QCM-D experiments is shown in fig. S1. Our control experiments have shown that the changes in Δf and ΔD displayed in Fig. 1A are not attributed to changes in bulk solution density and viscosity during solution exchange (figs. S2 and S3). Furthermore, Δf and ΔD of the PMETAC brushes at the other overtones have a similar pH dependence to those at the third overtone, further suggesting that the hydration and stiffness of the brushes are dependent on pH (fig. S4). Moreover, the water contact angle (WCA) and oil (1,2-dichloroethane) contact angle (OCA) of the PMETAC brushes can be reversibly tuned between ~7° and ~33° and between ~173° and ~155°, respectively, by changing the pH as illustrated in Fig. 1B. A similar WCA change obtained from the pendant bubble contact angle measurements and a similar OCA change of nonpolar oil can also be observed on the surface of PMETAC brushes (figs. S5 and S6).

The sliding velocity (V_s) of a poly(dimethylsiloxane) (PDMS) cylinder on the PMETAC brushes also shows strong pH dependence. It decreases from ~14.7 to ~0.04 cm s^{-1} as pH increases from 2 to 12, as shown in Fig. 1C, which implies that the friction force between the sliding block and the surface becomes larger when the pH is increased.

[1]Department of Chemical Physics, Hefei National Laboratory for Physical Sciences at the Microscale, University of Science and Technology of China, Hefei 230026, P. R. China. [2]Faculty of Materials Science and Engineering, South China University of Technology, Guangzhou 510640, P. R. China. [3]Department of Applied Mathematics, Research School of Physics and Engineering, Australian National University, Canberra, Australian Capital Territory 0200, Australia.
*Corresponding author. Email: gml@ustc.edu.cn (G.L.); msgzzhang@scut.edu.cn (G.Z.); shujiye@ustc.edu.cn (S.Y.); yiluo@ustc.edu.cn (Y.L.)

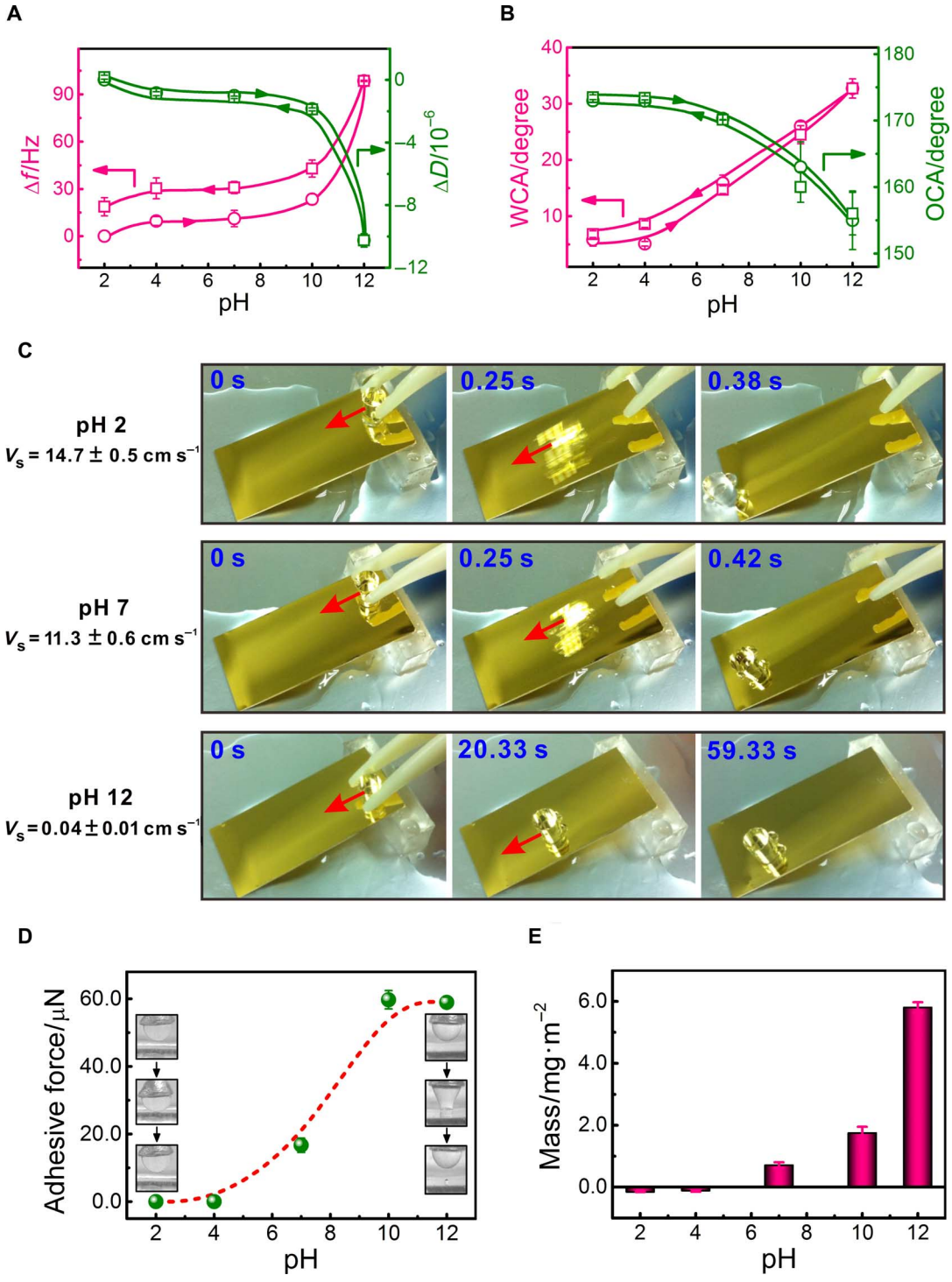

Fig. 1. Macroscopic pH-responsive properties of PMETAC brushes. The dry thickness of PMETAC brushes used here is ~26 ± 4 nm. (**A**) Shifts in frequency (Δf) and dissipation (ΔD) of PMETAC brushes as a function of pH at the overtone number (n) of 3. (**B**) Measured WCA and OCA on the surface of PMETAC brushes as a function of pH. (**C**) Lubrication tests on the surface of PMETAC brushes at different pH values. (**D**) The adhesive force between an oil (1,2-dichloroethane) droplet and the PMETAC brushes as a function of pH. Inset: A series of photos taken of the PMETAC brushes approaching and retracting from the oil droplet at pH 2 and 12 during measurements of the adhesive force. (**E**) The mass of adsorbed lysozyme on the PMETAC brushes as a function of pH. The mass was calculated from the frequency change induced by the lysozyme adsorption according to the Sauerbrey equation. Error bars are obtained from repeated measurements.

The lubrication tests can be viewed in movie S1. The adhesive force between an oil (1,2-dichloroethane) droplet and the PMETAC brushes follows similar pH dependence (Fig. 1D). It is observed that at pH 10 and 12, the oil droplet can be fully stretched until it ruptures, leaving behind a small residual oil droplet left on the surface (fig. S7). In this case, the measured force (~60.0 μN) corresponds to the stretching force, whereas the real adhesive force must be considerably larger. Likewise, protein adsorption on the PMETAC brushes can also be effectively modulated by pH (Fig. 1E and fig. S8).

Microscopic mechanism of pH response of positively charged SPBs

According to conventional wisdom, SPBs should be pH-insensitive because the average degree of charging of SP chains is independent of pH (*5*–*9*). As shown in Fig. 2A, the average degree of charging and the wet thickness of PMETAC brushes are independent of pH, as expected (*6*, *16*). The in situ atomic force microscopy (AFM) results further confirm that the wet thickness of the PMETAC brushes is independent of pH (fig. S9). However, all experimental evidence illustrated in Fig. 1 clearly indicates that such a simple fact cannot be generalized to other properties. To better understand these findings, we consider the Manning's counterion condensation theory, which states that SPs are not 100% dissociated, namely, a portion of counterions can be condensed onto the polyelectrolyte chains (*17*, *18*). As pH increases from 2 to 12, the concentration of OH^- increases from 10^{-12} to 10^{-2} M. Therefore, more OH^- will associate with the grafted PMETAC chains with increasing pH. The pH-dependent mole fraction of OH^- (f_{OH^-}) in the outer part of the PMETAC brushes obtained from x-ray photoelectron spectroscopy (XPS) measurements demonstrates increased adsorption of OH^- onto the brushes as pH increases (Fig. 2B and fig. S10). The pH-mediated hydroxide adsorption-desorption equilibrium with the brushes can be described by a Langmuir-type adsorption isotherm as shown in Fig. 2B (eq. S1).

The effect of pH on the cationic SPBs at the molecular scale was determined using surface-sensitive sum-frequency generation vibrational spectroscopy (SFG-VS) (*19*, *20*). The pH dependence of the SFG intensity of the interfacial water, as shown in Fig. 2C, directly confirms the dehydration of the cationic SPBs with increasing pH, consistent with the pH dependence of Δf displayed in Fig. 1A. Such behavior can be further illustrated by the change in strength of the 3200 cm^{-1} peak (fig. S11) and verified by the change in intensity of water signals in the ppp SFG spectra (fig. S12). Note that the contribution of the orientation change of the interfacial water molecules to the SFG intensity of water signals can be neglected here (figs. S11 and S12). The 1220 cm^{-1} spectral peak

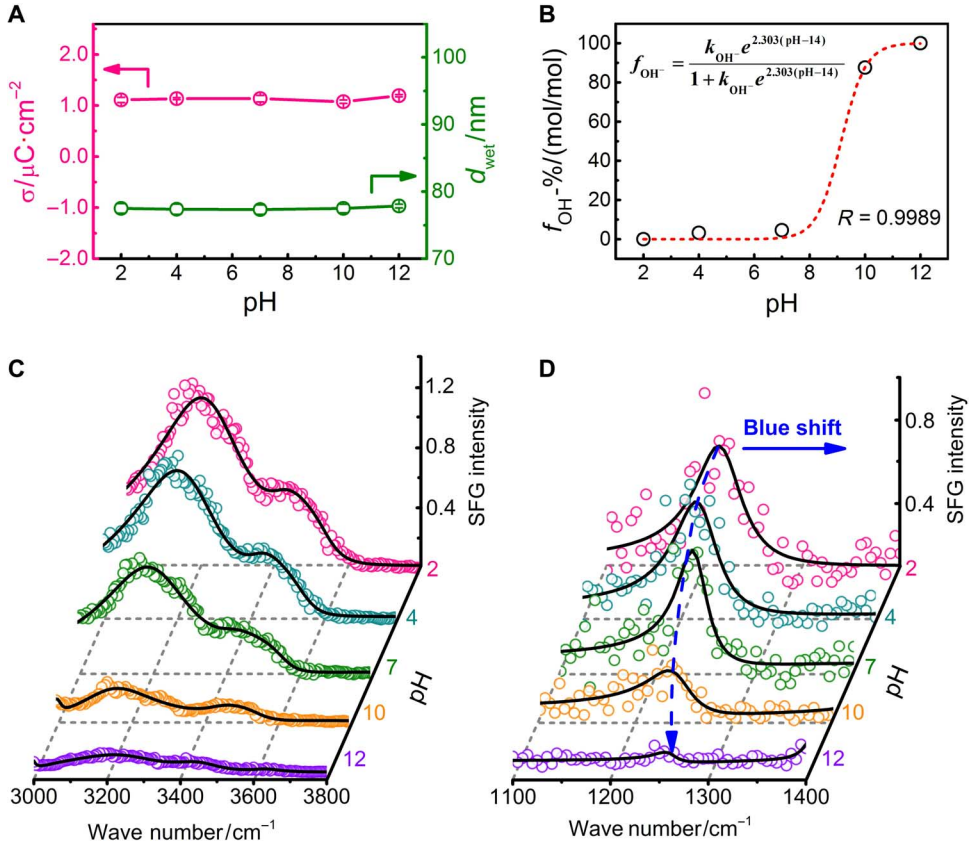

Fig. 2. Microscopic mechanism of pH response of PMETAC brushes. (**A**) Changes in surface charge density (σ) and wet thickness (d_{wet}) of the PMETAC brushes as a function of pH. (**B**) Change in mole fraction of OH^- (f_{OH^-}) in the outer part of the PMETAC brushes as a function of pH obtained from XPS measurements. The dashed line is a fit to the experimental data by the Langmuir-type adsorption isotherm. The equilibrium constant k_{OH^-} is determined by the ratio of the adsorption constant to the desorption constant of OH^-. (**C**) The ssp SFG spectra of PMETAC brushes in the frequency range of 3000 to 3800 cm^{-1} as a function of pH. (**D**) The ssp SFG spectra of PMETAC brushes in the frequency range of 1100 to 1400 cm^{-1} as a function of pH. Error bars are obtained from repeated measurements.

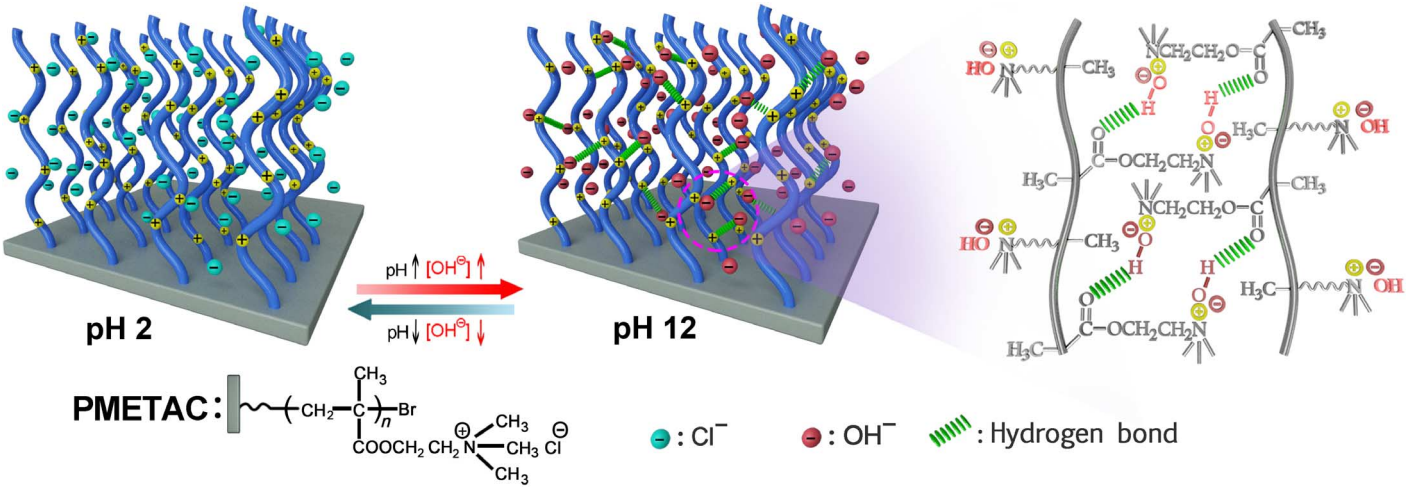

Fig. 3. Schematic illustration of the pH-mediated reorganization of the interchain hydrogen bond network of the PMETAC brushes. As pH increases, the interchain hydrogen bonds are formed between the grafted chains due to the adsorption of hydroxide onto the PMETAC brushes. For clarity, the K^+, H_3O^+, and excess free Cl^- and OH^- within the PMETAC brushes are not depicted in this figure.

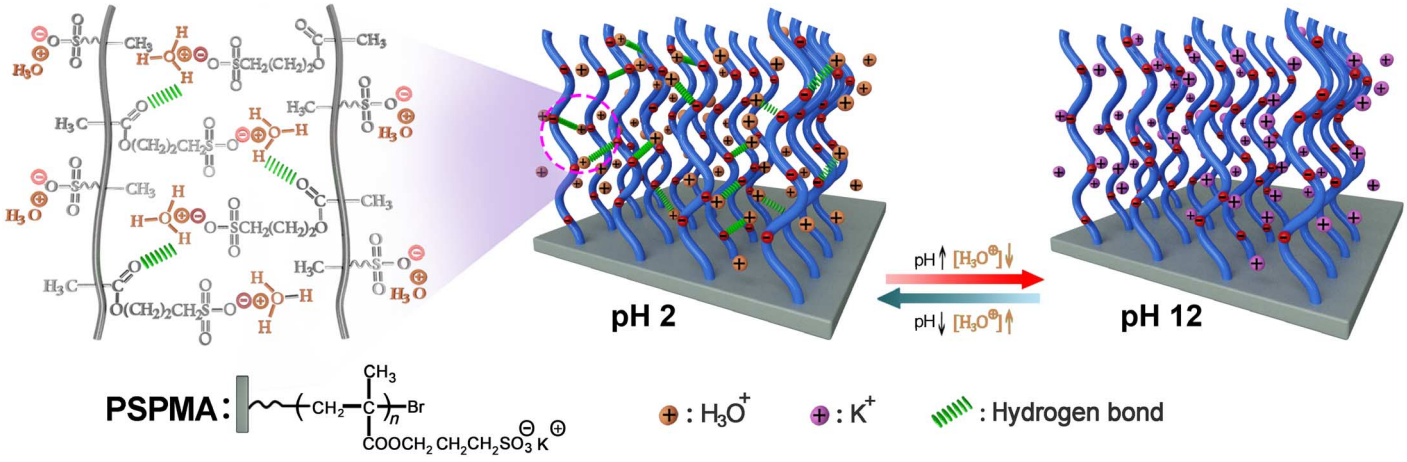

Fig. 4. Schematic illustration of the pH-mediated reorganization of the interchain hydrogen bond network of the PSPMA brushes. As pH increases, the interchain hydrogen bonds are broken between the grafted chains due to the desorption of hydronium from the PSPMA brushes. For clarity, the Cl^-, OH^-, and excess free K^+ and H_3O^+ within the PSPMA brushes are not depicted in this figure.

corresponds to the C–O stretching in the –C(=O)OR side group. This peak appears in the ssp spectra in Fig. 2D but is completely absent in the ppp spectra (fig. S13). This fact indicates that the transition dipole direction of the C–O stretching lies more parallelly with the surface. The 1220 cm^{-1} peak shifts to higher frequency at higher pH values (fig. S14), suggesting that the neighboring chains form interchain hydrogen bonds through the bound hydroxide and the carbonyl of the –C(=O)OR group, which is accompanied by the shortening of the C–O bond. Furthermore, the decrease in C–O peak intensity with increasing pH implies an increased C–O symmetry due to the rotation of certain –C(=O)OR groups to form interchain hydrogen bonds following the adsorption of OH^- (fig. S15). The formation of interchain hydrogen bonds and the rearrangement of chain conformations with pH are further validated by changes in C=O stretching, $–CH_2–$ symmetric stretching, and symmetric stretching of the $–CH_3$ group connected with the polymer backbone (figs. S16 to S18).

The pH-mediated reorganization of the interchain hydrogen bond network of the PMETAC brushes is schematically illustrated in Fig. 3. Almost no interchain hydrogen bonds can be formed between the grafted chains at pH 2 because of the absence of hydrogen bond donors associated with the grafted chains. As pH increases, the neighboring chains start to form interchain hydrogen bonds through the bound hydroxide and the carbonyl. The formation of interchain hydrogen bonds weakens the interactions between the cationic SPBs and the surrounding water molecules, resulting in the dehydration of PMETAC brushes with increasing pH. The interchain hydrogen bonding can physically crosslink the brushes, making them stiffer with increasing pH. Similarly, the observed pH dependencies of the WCA, OCA, friction force, adhesive force, and protein adsorption can also be correlated with the change in hydration of the PMETAC brushes induced by the reorganization of the interchain hydrogen bond network (*11*, *21*–*23*).

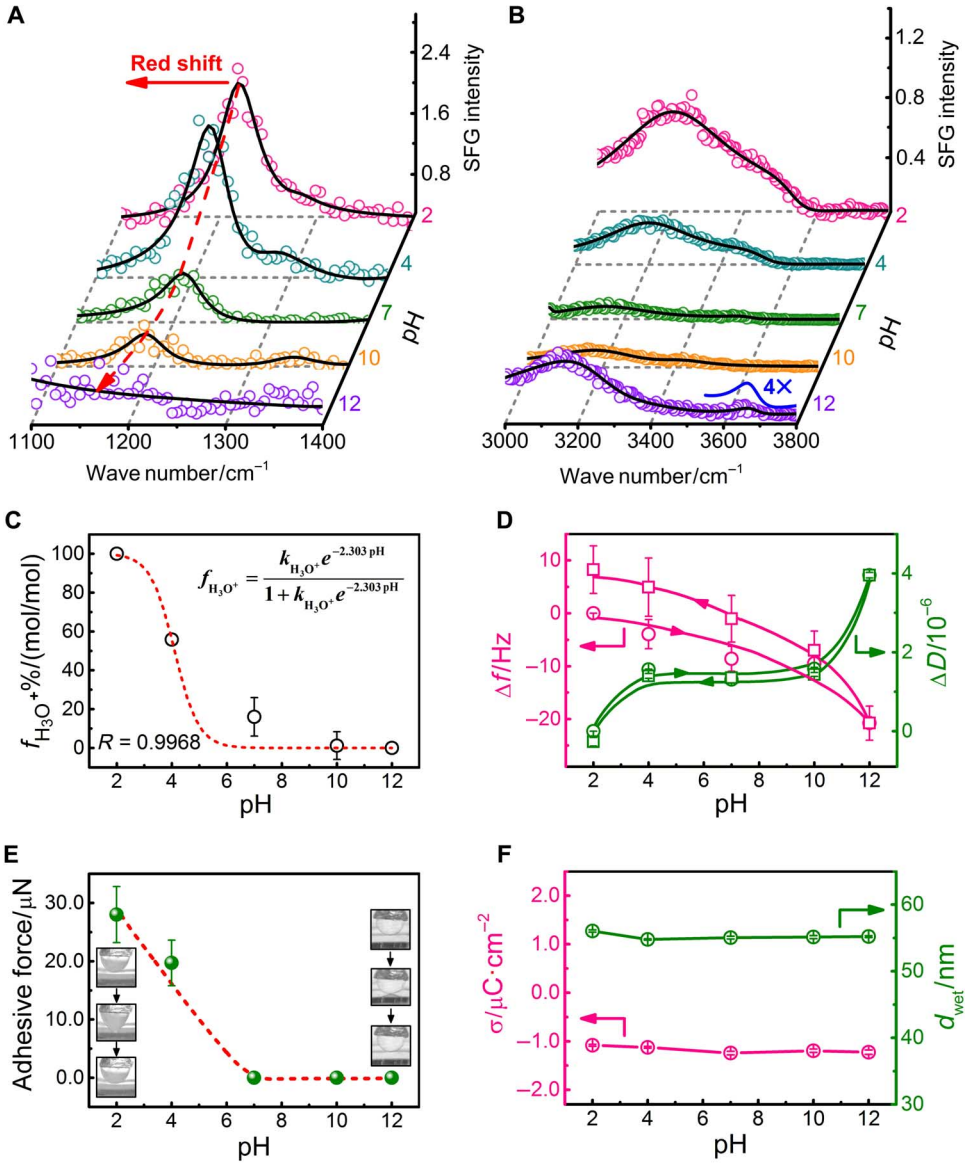

Fig. 5. pH response of PSPMA brushes. The dry thickness of the PSPMA brushes used here is ~26 ± 4 nm. (**A**) The ppp SFG spectra of PSPMA brushes in the frequency range of 1100 to 1400 cm^{-1} as a function of pH. (**B**) The ssp SFG spectra of PSPMA brushes in the frequency range of 3000 to 3800 cm^{-1} as a function of pH. (**C**) Change in mole fraction of H_3O^+ ($f_{H_3O^+}$) in the outer part of the PSPMA brushes as a function of pH obtained from XPS measurements. The dashed line is a fit to the experimental data by the Langmuir-type adsorption isotherm. The equilibrium constant $k_{H_3O^+}$ is determined by the ratio of the adsorption constant to the desorption constant of H_3O^+. (**D**) Shifts in frequency (Δf) and dissipation (ΔD) of the PSPMA brushes as a function of pH at the overtone number (n) of 3. (**E**) The adhesive force between an oil (1,2-dichloroethane) droplet and the PSPMA brushes as a function of pH. Inset: A series of photos taken at pH 2 and 12 during measurements of the adhesive force. (**F**) Changes in surface charge density (σ) and wet thickness (d_{wet}) of the PSPMA brushes as a function of pH. Error bars are obtained from repeated measurements.

pH response of negatively charged SPBs

The concept of pH-mediated reorganization of the interchain hydrogen bond network can be directly applied to anionic PSPMA brushes as shown in Fig. 4. Generally, the proton exists in the form of hydronium (H_3O^+) in aqueous solutions (*24*). The increase of pH results in the desorption of the bound H_3O^+ from the PSPMA brushes as the concentration of H_3O^+ decreases from 10^{-2} to 10^{-12} M, when pH increases from 2 to 12. Consequently, the interchain hydrogen bonds formed between the bound H_3O^+ and the carbonyl of the –C(=O)OR group at pH 2 should be gradually broken, and the C–O peak in the SFG spectra is expected to shift to lower frequency with increasing pH.

The predicted reorganization of the interchain hydrogen bond network of the PSPMA brushes is confirmed by the SFG spectra shown in Fig. 5A, in which the C–O bond is lengthened, indicated by a lower stretching frequency with increasing pH (fig. S19). The more perpendicular orientation of the C–O bond to the surface is verified by the fact

that the 1220 cm^{-1} peak can be readily observed in the ppp spectra but is completely absent in the ssp spectra (fig. S20). This suggests that the reorganization of the interchain hydrogen bond network of the PSPMA brushes is slightly different from that of the PMETAC brushes. The reduction in the strength of the 1220 cm^{-1} peak with increasing pH implies an increased C–O symmetry during the breaking of the interchain hydrogen bonds (fig. S21). The chain rearrangement with pH is further validated by changes in spectral features of the $-CH_3$ and $-CH_2-$ groups (fig. S22).

Simultaneously, the decrease of the SFG water signals with the increase of pH from 2 to 10, as shown in Fig. 5B, is due to the desorption of H_3O^+. As pH increases from 10 to 12, the increase in water signals is attributed to the formation of interwater hydrogen bonds in the hydration shell of the OH^- ion [$OH^-(H_2O)_n$] associated with bound K^+, which is confirmed by the appearance of an additional small band at 3680 cm^{-1} at pH 12 (*25*, *26*). The change in water signals is further verified by variations in the strength of the 3200 cm^{-1} peak (fig. S23) and in the intensity of water signals in the ppp SFG spectra (fig. S24).

Moreover, the pH-mediated hydronium adsorption-desorption equilibrium with the brushes is confirmed by XPS measurements (fig. S25) and can be described by a Langmuir-type adsorption isotherm as presented in Fig. 5C (eq. S3). The changes in hydration and stiffness of the PSPMA brushes with pH, as reflected by the pH-dependent Δf and ΔD at the third overtone (Fig. 5D) and at the other overtones (fig. S26), as well as the pH dependence of the adhesive force of the PSPMA brushes (Fig. 5E) are all attributed to the pH-mediated reorganization of the interchain hydrogen bond network. Again, the observed pH response is unrelated to the average degree of charging and wet thickness of the anionic SPBs (Fig. 5F and fig. S27). The smaller change in Δf of the PSPMA brushes compared with that of the PMETAC brushes indicates that the reorganization of the hydrogen bond network has a relatively weak influence on the hydration of the former than that of the latter, thereby resulting in a weak pH effect on the surface wettability and lubricity of the PSPMA brushes (figs. S28 to S31 and movie S2). This may be due to the fact that the sulfonate group has enough hydrogen bond acceptors (that is, three oxygen atoms) to interact with the surrounding water molecules during reorganization of the hydrogen bond network.

DISCUSSION

Note that the pH response of weak polyelectrolyte brushes originates from the variation in the degree of charging of weak polyelectrolyte chains, which is determined by the pH-controlled proton association-dissociation equilibrium of acidic or basic groups (figs. S32 to S36), whereas the reorganization of the interchain hydrogen bond network triggered by the pH-mediated adsorption-desorption equilibrium of hydronium or hydroxide (that is, hydrogen bond donors) with the brushes observed here determines the pH-responsive properties of SPBs. These pH effects are common because hydrogen bond acceptors are ubiquitous in SP systems (*27*, *28*). We emphasize that the pH effect of SPBs demonstrated here has different origins and applications compared to conventional ion exchange materials (*29*). We have demonstrated that the properties of SPBs are insensitive to a simple ion exchange at a constant pH value (fig. S37). Furthermore, we have also demonstrated that the pH response of SPBs observed here is not induced by specific ion effects (fig. S38). Naturally, the pH-responsive SPBs that allow a range of properties to be modulated over a wide pH range are more desirable for applications in biological fields (*30*). In addition, we have found that free SPs are also pH-responsive, owing to the same underlying mechanism (fig. S39). The detailed understanding of the mechanism elucidated here provides a platform for utilizing and controlling the pH response of SPBs as a new class of smart materials. Because pH is a fundamentally important measure of aqueous solutions and hydrogen bonding is ubiquitous in both artificial and biological polyelectrolyte systems, we believe that our findings will markedly expand the range of applications of SPBs and inspire new ideas for building novel smart materials by enabling SPBs to be used as pH-responsive units.

MATERIALS AND METHODS

Materials

[2-(Methacryloyloxy)ethyl]trimethylammonium chloride (METAC) [75 weight % (wt %) in H_2O; Aladdin] and 2-(dimethyl amino)ethyl methacrylate (DMAEMA) (99%; Aladdin) were purified by passing through a basic alumina column (200 to 300 mesh). Ethyl methacrylate (EMA) (99%; Aladdin) was purified by treatment with 5% aqueous NaOH solution to remove the inhibitor and was distilled under vacuum. Sodium methacrylate (MA) (99%; Aladdin), potassium 3-sulfopropyl methacrylate (SPMA) (98%; Sigma-Aldrich), and vinylbenzyl trimethylammonium chloride (VBTMA) (97%; Acros) were used as received. 1,1,4,7,10,10-Hexamethyltriethylenetetramine (HMTETA) (97%; Energy Chemical), 2,2′-dipyridyl (BPy) (>99%; Aldrich), copper (II) bromide ($CuBr_2$) (99%; Alfa Aesar), copper (II) chloride ($CuCl_2$) (98%; Alfa Aesar), ethyl 2-bromoisobutyrate (2-EBiB) (98%; Aldrich), methanol (≥99.9%) (for high-performance liquid chromatography), and *N*,*N*′-dimethylformamide (DMF) (≥99.9%; Aladdin) (for gas chromatography) were used as received. 1,1,4,7,7-Pentamethyldiethylenetriamine (PMDETA) (98%; Aladdin) was purified by distillation under vacuum. Copper (I) bromide (CuBr) and copper (I) chloride (CuCl) were prepared from $CuBr_2$ and $CuCl_2$, respectively, by reaction with sodium sulfite. ω-Mercaptoundecyl bromoisobutyrate (MUBB) (98%; Beijing HRBio Biotechnology Co.), HCl (37 wt %, ultra pure; Jincheng Chemical), lysozyme (Calbiochem), and 1,2-dichloroethane (AR, Sinopharm) were used as received. Hexadecane (anhydrous, ≥99%; Aladdin) was purified by filtering through a neutral alumina column to remove trace amounts of surfactant. All salts (99.99%, metals basis) were purchased from Aladdin and used as received. Water was purified by filtration through a Millipore gradient system after distillation, giving a resistivity of 18.2 megaohm·cm.

Preparation of polymer brushes

The gold-coated resonators used in the QCM-D were cleaned by piranha solution [H_2O_2/H_2SO_4, 3:7 (v/v)] for 10 min at 60°C, then rinsed with copious amounts of Milli-Q water, and dried under a nitrogen stream before use. The clean resonators were immersed in a 5 mM solution of MUBB in anhydrous ethanol for ~24 hours at room temperature to form a uniform monolayer of initiator with a thickness of ~1.2 nm, as determined by ellipsometry.

According to the procedures reported previously, PMETAC and PSPMA brushes were prepared using the SI-ATRP method (*31*). Typically, METAC (5.94 g, 28.6 mmol), the free initiator 2-EBiB (0.027 g,

0.14 mmol), and BPy (0.044 g, 0.28 mmol) were dissolved in 20 ml of methanol/water mixture [4:1 (v/v)]. Then, the initiator-modified substrates were placed inside the flask, and the solution was stirred at 25°C under argon for 120 min to remove dissolved oxygen. Afterward, CuBr (0.02 g, 0.14 mmol) and $CuBr_2$ (0.003 g, 0.014 mmol) were quickly added under argon protection at 25°C. The polymerization was allowed to proceed for a specific time to prepare the PMETAC brushes. At the end of polymerization, the resonators grafted with PMETAC brushes were washed with water and methanol, and then soaked in a methanol/water mixture [4:1 (v/v)] overnight to remove the ligand and unreacted monomer. Likewise, PSPMA brushes were grafted onto surfaces as follows. Briefly, SPMA (4.93 g, 20 mmol), 2-EBiB (0.02 g, 0.1 mmol), CuBr (0.016 g, 0.11 mmol), $CuBr_2$ (0.0025 g, 0.011 mmol), and BPy (0.034 g, 0.22 mmol) were dissolved in 20 ml of DMF/water mixture [1:1 (v/v)] for preparation of the PSPMA brushes. After the polymerization, the resonators grafted with PSPMA brushes were washed with DMF/water mixture [1:1 (v/v)], and then soaked in 0.5 wt % EDTA-2Na aqueous solution overnight to remove the ligand and unreacted monomer. The grafting density (σ) of both PMETAC and PSPMA brushes was ~0.4 chains/nm^2, estimated according to the equation $\sigma = \rho d_{dry} N_A / M_n$, where ρ is the density of the brushes (~1.1 g/cm^3), d_{dry} is the dry thickness of the brushes, M_n is the number-average molar mass of the polyelectrolyte chains determined by gel permeation chromatography, and N_A is the Avogadro constant.

Preparation of pH solutions

Solutions with different pH values but the same ionic strength were prepared using 10 mM HCl, 10 mM KOH, and 10 mM KCl for investigation of the pH-responsive properties of SPBs. More specifically, the solutions of pH 2 and 12 were prepared using 10 mM HCl and 10 mM KOH, respectively. The solutions of pH 4, 7, and 10 were prepared by adding a small amount of 10 mM HCl or 10 mM KOH to 10 mM KCl to obtain target pH values with the same ionic strength. Buffered pH solutions were not used here to avoid the generation of specific ion effects (*32*).

In situ combination of QCM-D and ellipsometry measurements

The pH-responsive behaviors of polymer brushes in aqueous solutions were investigated by the combination of QCM-D and spectroscopic ellipsometry (SE) with an ellipsometry-compatible QCM-D module (QELM 401) from Q-Sense AB (*33*). The quartz crystal resonator with a fundamental resonant frequency of 5 MHz was mounted in a fluid cell with one side exposed to the solution. The resonator had a mass sensitivity constant (C) of 17.7 ng·cm^{-2}·Hz^{-1}. When a quartz crystal is excited to oscillate in the thickness shear mode at its fundamental resonant frequency (f_0) by applying a radio frequency voltage across the electrodes near the resonant frequency, a small layer added to the electrodes induces a decrease in resonant frequency (Δf), which is proportional to the mass change (Δm) of the layer. Under vacuum or in air, if the added layer is rigid, evenly distributed, and much thinner than the crystal, then the Δf is related to Δm and the overtone number (n = 1, 3, 5….) by the Sauerbrey equation (*14*)

$$\Delta m = -\frac{\rho_q l_q}{f_0}\frac{\Delta f}{n} = -C\frac{\Delta f}{n} \quad (1)$$

where f_0 is the fundamental frequency, and ρ_q and l_q are the specific density and thickness of the quartz crystal, respectively. The dissipation factor is defined by (*33*)

$$D = \frac{E_d}{2\pi E_s} \quad (2)$$

where E_d is the energy dissipated during one oscillation, and E_s is the energy stored in the oscillating system. The measurement of ΔD is based on the fact that the voltage over the crystal decays exponentially as a damped sinusoidal when the driving power of a piezoelectric oscillator is switched off (*33*). By periodically switching the driving voltage on and off, a series of measures of the resonant frequency and the dissipation factor can simultaneously be obtained. In the QCM-D studies on the pH response of polymer brushes, the changes in Δf and ΔD were obtained by taking the absolute values of frequency and dissipation at pH 2 as the reference. All the experiments were conducted at 25° ± 0.02°C.

The thicknesses of the brushes in both dry and wet states were determined by a spectroscopic ellipsometer (M-2000V, J. A. Woollam). The dry thickness of the brushes was determined at two incident angles in air. The wet thickness of the brushes was determined at the incident angle of 65° in pH solutions using an ellipsometry-compatible QCM-D module. Ellipsometric measurements are sensitive to the change in polarization state of light reflected from a surface, whereas the two ellipsometric parameters Ψ and Δ are recorded and can be expressed by the following equation (*34*)

$$\tan(\Psi)e^{i\Delta} = \frac{R_p}{R_s} \quad (3)$$

where tan(Ψ) is the amplitude ratio of the reflection coefficient of p-polarized light (R_p) to that of s-polarized light (R_s), and Δ is the phase difference. The quantities Ψ and Δ were measured directly in experiments, and the physical parameters, such as thickness and refractive index, can be obtained by numerical fitting using an appropriate model.

The dry thickness of the polymer brushes was determined by numerical fitting using the software CompleteEASE (J. A. Woollam) by treating the polymer layer as a single Cauchy layer between the gold surface and air. With this model, the refractive index of the substances follows the relation of $n = A_n + (B_n/\lambda^2)$, where n is the refractive index, A_n and B_n are the two fitting parameters related to n, and λ is the wavelength of incident light. To measure the dry thickness of the polymer brushes, the refractive indices of the PMETAC (A_n = 1.495 and B_n = 0.01) and PSPMA (A_n = 1.46 and B_n = 0.01) brushes were assumed to be described by the Cauchy parameters (*35*, *36*). The optical properties of the resonator's gold surface were fit with a B-spline function and fixed during modeling of the polymer layer. The wet thickness of the polymer brushes was determined by numerical modeling of the ellipsometric data with a two-layer model using the software CompleteEASE. The pH solutions with the blank gold-coated resonator were at first recorded as the background signals. The two layers represented the polymer layer and the gold coating. The swollen polymer layer was treated as a single layer, which was assumed to be transparent and homogeneous (Cauchy medium). The refractive index and the

wet thickness of the brushes can be obtained simultaneously by numerical fitting of the ellipsometric data (*37*). In this work, all dry and wet thicknesses of the polymer brushes were determined by SE unless mentioned specifically.

SFG-VS measurements

SFG-VS is a second-order nonlinear optical spectroscopic technique that has submonolayer surface sensitivity. Here, all SFG experiments were carried out at ~25°C. SFG spectra from the interfacial molecules with different polarization combinations including ssp [s-polarized SF output, s-polarized visible input, and p-polarized infrared (IR) input] and ppp were collected using the near-total internal reflection geometry with two input laser beams traveling through a ~4-nm SiO_2 layer–coated CaF_2 prism and overlapping on the polymer/aqueous solution interface. The PMETAC brushes with a dry thickness of ~25 nm and the PSPMA brushes with a dry thickness of ~22 nm were grafted on the SiO_2 surface using the SI-ATRP method. All SFG spectra were normalized by the intensities of the input IR and visible beams. SFG spectra were recorded from the brushes/aqueous solution interface after the sample was placed in the solutions at different pH values to equilibrate for at least 20 min.

As described in detail elsewhere, the intensity of the SFG light is related to the square of the sample's second-order nonlinear susceptibility $\chi^{(2)}_{\text{eff}}$ and the intensity of the two input fields $I(\omega_{\text{IR}})$ and $I(\omega_{\text{vis}})$ (see Eq. 4), which vanishes when a material has inversion symmetry (*19*)

$$I(\omega_{\text{SFG}}) \propto \left|\chi^{(2)}_{\text{eff}}\right|^2 I_1(\omega_{\text{vis}}) I_2(\omega_{\text{IR}}) \tag{4}$$

where $\omega_{\text{SFG}} = \omega_{\text{IR}} + \omega_{\text{vis}}$. As the IR beam frequency is tuned over the vibrational resonance of molecules at interfaces, the effective surface nonlinear susceptibility $\chi^{(2)}_{\text{R}}$ can be enhanced. The frequency dependence of $\chi^{(2)}_{\text{eff}}$ is described by

$$\chi^{(2)}_{\text{eff}}(\omega) = \chi^{(2)}_{\text{NR}} + \sum_{\upsilon} \frac{A_\upsilon}{\omega - \omega_\upsilon + i\Gamma_\upsilon} \tag{5}$$

where A_υ, ω_υ, and Γ_υ are the strength, resonant frequency, and damping coefficient of the vibrational mode (υ), respectively. A_υ could be either positive or negative depending on the phase of the vibrational mode (*19*). The plot of SFG signal versus IR input frequency shows a polarized vibrational spectrum of the molecules at the interface. A_υ, ω_υ, and Γ_υ can be extracted by fitting the spectrum.

ζ potential measurements

The surface ζ potential of polymer brushes was measured using a DelsaNano C particle and ζ potential analyzer with a specially designed flat surface cell (Beckman Coulter). ζ is obtained according to the Smoluchowski equation (*38*),

$$\zeta = \frac{4\pi\eta U}{\varepsilon} \tag{6}$$

where U is the electrophoretic mobility, η is the viscosity of solution, and ε is the dielectric constant of solution. One can also obtain the surface charge density (σ) from ζ on the basis of the Grahame equation (*39*)

$$\sigma = \sqrt{8\varepsilon\varepsilon_0 RTc}\ \sinh\left(\frac{zF\zeta}{2RT}\right) \tag{7}$$

where R is the gas constant, T is temperature, F is the Faraday constant, z is the valence of counterion, ε_0 is the permittivity of vacuum, and c is the concentration of electrolyte solution.

The clean quartz slides were immersed in a 10 mM toluene solution of [3-(2-bromoisobutyryl)propyl]triethoxysilane for 16 hours at room temperature to form a monolayer of initiator. Afterward, the polymer brushes were formed by polymerization using SI-ATRP. The quartz slide grafted with the polymer brushes was fixed onto the flat surface cell to conduct the measurements.

Contact angle measurements

The static WCAs and OCAs on the surfaces of PMETAC and PSPMA brushes were determined using a KSV CAM 200 contact angle goniometer at 25°C. The polyelectrolyte brushes were soaked in the relevant pH solutions for ~20 min and then rinsed with water and dried with N_2 before each WCA measurement. The OCA and pendant bubble contact angle measurements on the surface of polyelectrolyte brushes were performed in the relevant pH solutions.

Adhesive force measurements

The adhesive force was measured using a high-sensitivity microelectromechanical balance system (DataPhysics DCAT 11) underwater at room temperature. A dichloroethane droplet (10 μl) was suspended from a metal cap. The substrate was placed on the balance table and immersed in the relevant pH solutions. The substrate was moved upward at a constant speed of 0.1 mm s^{-1}, until the substrate contacted the oil droplet, and the substrate was then retracted from the oil droplet. The force was recorded during the entire cycle and used to determine the adhesive force.

XPS measurements

XPS measurements of the PMETAC and PSPMA brushes grafted on gold-coated silicon wafers were performed on an x-ray photoelectron spectrometer (ESCALAB 250, Thermo-VG Scientific Corporation) using a monochromatic focused Al Kα x-ray source (1486.6 eV). Each surface was soaked in the relevant pH solutions for ~20 min and then rinsed with water to remove physically adsorbed salts and dried with a stream of nitrogen gas before XPS measurements. No physically adsorbed salts could be detected, as shown in fig. S40, indicating that the signal of Cl^- for the cationic SPBs solely resulted from the counterions of PMETAC brushes and that the signal of K^+ for the anionic SPBs solely resulted from the counterions of PSPMA brushes during XPS measurements. The peak assignment of elements was referred to the NIST XPS Database, and all spectra were calibrated with the C_{1s} peak at 284.6 eV.

Lubrication tests

Qualitative macroscopic lubrication tests were performed on a gold surface grafted with SPBs by using an elastomeric PDMS cylinder with a diameter of 6 mm as a sliding block at different pH values, as in a previous study (*40*). The angle of inclination of the surface was fixed at ~10°. The PDMS block was allowed to slide on the surface from the

top to the bottom in the presence of Milli-Q water. The SPBs were soaked in the relevant pH solutions for ~20 min and then rinsed with water and dried with N_2 before each lubrication test. Note that the corresponding pH-dependent properties of the SPBs would be retained after rinsing the samples with water and drying with N_2 (fig. S31).

SUPPLEMENTARY MATERIALS

Supplementary material for this article is available at http://advances.sciencemag.org/cgi/content/full/2/8/e1600579/DC1

fig. S1. The time scale for the pH-responsive behavior of the PMETAC brushes in QCM-D experiments, where the overtone number (*n*) is 3.
fig. S2. Δf and ΔD as a function of pH of the blank gold-coated resonator, where the overtone number (*n*) is 3.
fig. S3. Shifts in frequency (Δf) and dissipation (ΔD) as a function of pH of the gold-coated resonator grafted with PEMA brushes, where the overtone number (*n*) is 3.
fig. S4. Δf and ΔD as a function of pH of the gold-coated resonator grafted with PMETAC brushes at the overtone number (*n*) of 3, 5, and 7.
fig. S5. WCA on the surface of PMETAC brushes as a function of pH obtained from the pendant bubble contact angle measurements under the relevant pH solutions.
fig. S6. Measured oil (hexadecane) contact angle (OCA) on the surface of PMETAC brushes as a function of pH.
fig. S7. A series of photos taken of the PMETAC brushes approaching and retracting from an oil (1,2-dichloroethane) droplet at different pH values during measurements of the adhesive force.
fig. S8. Δf and ΔD induced by protein adsorption on the surface of PMETAC brushes as a function of pH.
fig. S9. In situ AFM measurements of the wet thickness of the PMETAC brushes with pH.
fig. S10. XPS measurements of the PMETAC brushes as a function of pH.
fig. S11. Change in fitting strength of the 3200 cm^{-1} peak of the PMETAC brushes as a function of pH in the ssp SFG spectra.
fig. S12. The ppp SFG spectra of PMETAC brushes in the frequency range of 3000 to 3800 cm^{-1} as a function of pH.
fig. S13. The ppp SFG spectra of PMETAC brushes in the frequency range of 1100 to 1400 cm^{-1} as a function of pH.
fig. S14. Change in frequency of the C–O stretching peak of the PMETAC brushes as a function of pH in the ssp SFG spectra.
fig. S15. Change in fitting strength of the 1220 cm^{-1} peak of the PMETAC brushes as a function of pH in the ssp SFG spectra.
fig. S16. The ssp SFG spectra of the PMETAC brushes in the frequency range of 2750 to 3100 cm^{-1} as a function of pH.
fig. S17. The ppp SFG spectra of the PMETAC brushes in the frequency range of 1600 to 1800 cm^{-1} as a function of pH.
fig. S18. The ssp SFG spectra of the PMETAC brushes in the frequency range of 1600 to 1800 cm^{-1} as a function of pH.
fig. S19. Change in frequency of the C–O stretching peak of the PSPMA brushes as a function of pH in the ppp SFG spectra.
fig. S20. The ssp SFG spectra of the PSPMA brushes in the frequency range of 1100 to 1400 cm^{-1} as a function of pH.
fig. S21. Change in fitting strength of the 1220 cm^{-1} peak of the PSPMA brushes as a function of pH in the ppp SFG spectra.
fig. S22. The ppp SFG spectra of the PSPMA brushes in the frequency range of 1400 to 1800 cm^{-1} as a function of pH.
fig. S23. Change in fitting strength of the 3200 cm^{-1} peak of the PSPMA brushes as a function of pH in the ssp SFG spectra.
fig. S24. The ppp SFG spectra of PSPMA brushes in the frequency range of 3000 to 3800 cm^{-1} as a function of pH.
fig. S25. XPS measurements of the PSPMA brushes as a function of pH.
fig. S26. Δf and ΔD as a function of pH of the gold-coated resonator grafted with PSPMA brushes at the overtone number (*n*) of 3, 5, and 7.
fig. S27. In situ AFM measurements of the wet thickness of the PSPMA brushes with pH.
fig. S28. Water contact angle (WCA) on the surface of PSPMA brushes as a function of pH obtained from the contact angle measurements in air.
fig. S29. WCA on the surface of PSPMA brushes as a function of pH obtained from the pendant bubble contact angle measurements under the relevant pH solutions.
fig. S30. OCA on the surface of PSPMA brushes as a function of pH.
fig. S31. Lubrication tests on the surface of PSPMA brushes at different pH values.
fig. S32. Surface ζ potential and surface charge density (s) as a function of pH for the blank substrate and the quartz substrates grafted with PMETAC, PSPMA, PDMAEMA, and PMA brushes.
fig. S33. Δf and ΔD of the gold-coated resonator grafted with PMA brushes as a function of pH, where the overtone number (*n*) is 3.
fig. S34. Wet thickness of the PMA brushes as a function of pH obtained from ellipsometric measurements.
fig. S35. Δf and ΔD of the gold-coated resonator grafted with PDMAEMA brushes as a function of pH, where the overtone number (*n*) is 3.
fig. S36. Wet thickness of the PDMAEMA brushes as a function of pH obtained from ellipsometric measurements.
fig. S37. Response of the PMETAC brushes as a function of the concentration of OH^- or Br^-.
fig. S38. Response of the PMETAC and PVBTMA brushes as a function of pH.
fig. S39. Molar conductivity (Λ_m) of free strong polyelectrolytes as a function of pH at different polymer concentrations.
fig. S40. XPS spectra of the PMETAC and PSPMA brushes as a function of pH.
movie S1. Lubrication tests on the surface of PMETAC brushes at different pH values.
movie S2. Lubrication tests on the surface of PSPMA brushes at different pH values.
References (*41*–*50*)

REFERENCES AND NOTES

1. G. Wee, O. Larsson, M. Srinivasan, M. Berggren, X. Crispin, S. Mhaisalkar, Effect of the ionic conductivity on the performance of polyelectrolyte-based supercapacitors. *Adv. Funct. Mater.* **20**, 4344–4350 (2010).
2. D. Rana, T. Matsuura, Surface modifications for antifouling membranes. *Chem. Rev.* **110**, 2448–2471 (2010).
3. T. Boudou, T. Crouzier, K. Ren, G. Blin, C. Picart, Multiple functionalities of polyelectrolyte multilayer films: New biomedical applications. *Adv. Mater.* **22**, 441–467 (2010).
4. L. Dong, A. K. Agarwal, D. J. Beebe, H. Jiang, Adaptive liquid microlenses activated by stimuli-responsive hydrogels. *Nature* **442**, 551–554 (2006).
5. M. A. C. Stuart, W. T. S. Huck, J. Genzer, M. Müller, C. Ober, M. Stamm, G. B. Sukhorukov, I. Szleifer, V. V. Tsukruk, M. Urban, F. Winnik, S. Zauscher, I. Luzinov, S. Minko, Emerging applications of stimuli-responsive polymer materials. *Nat. Mater.* **9**, 101–113 (2010).
6. S. Mura, J. Nicolas, P. Couvreur, Stimuli-responsive nanocarriers for drug delivery. *Nat. Mater.* **12**, 991–1003 (2013).
7. I. Cobo, M. Li, B. S. Sumerlin, S. Perrier, Smart hybrid materials by conjugation of responsive polymers to biomacromolecules. *Nat. Mater.* **14**, 143–159 (2015).
8. J.-L. Barrat, J.-F. Joanny, Theory of polyelectrolyte solutions. In *Advances in Chemical Physics*, I. Prigorin, S. A. Rice, Eds. (Wiley, Hoboken, NJ, 1996), vol. 94.
9. M. Schmidt, *Polyelectrolytes with Defined Molecular Architecture I* (Springer, Berlin-Heidelberg, 2004).
10. B. M. L. Dioos, I. F. J. Vankelecom, P. A. Jacobs, Aspects of immobilisation of catalysts on polymeric supports. *Adv. Synth. Catal.* **348**, 1413–1446 (2006).
11. U. Raviv, S. Giasson, N. Kampf, J.-F. Gohy, R. Jérôme, J. Klein, Lubrication by charged polymers. *Nature* **425**, 163–165 (2003).
12. M. Raftari, Z. J. Zhang, S. R. Carter, G. J. Leggett, M. Geoghegan, Nanoscale contact mechanics between two grafted polyelectrolyte surfaces. *Macromolecules* **48**, 6272–6279 (2015).
13. J. Tang, M. F. X. Lee, W. Zhang, B. Zhao, R. M. Berry, K. C. Tam, Dual responsive pickering emulsion stabilized by poly[2-(dimethylamino)ethyl methacrylate] grafted cellulose nanocrystals. *Biomacromolecules* **15**, 3052–3060 (2014).
14. G. Sauerbrey, Verwendung von Schwingquarzen zur Wägung dünner Schichten und zur Mikrowägung. *Z. Phys.* **155**, 206–222 (1959).
15. N.-J. Cho, C. W. Frank, B. Kasemo, F. Höök, Quartz crystal microbalance with dissipation monitoring of supported lipid bilayers on various substrates. *Nat. Protoc.* **5**, 1096–1106 (2010).
16. R. Förch, H. Schönherr, A. T. A. Jenkins, *Surface Design: Applications in Bioscience and Nanotechnology* (John Wiley & Sons, Weinheim, 2009).
17. G. S. Manning, Limiting laws and counterion condensation in polyelectrolyte solutions I. Colligative properties. *J. Chem. Phys.* **51**, 924–933 (1969).
18. E. Trizac, G. Téllez, Onsager-Manning-Oosawa condensation phenomenon and the effect of salt. *Phys. Rev. Lett.* **96**, 038302 (2006).
19. Z. Chen, Y. R. Shen, G. A. Somorjai, Studies of polymer surfaces by sum frequency generation vibrational spectroscopy. *Annu. Rev. Phys. Chem.* **53**, 437–465 (2002).
20. Z. Chen, Investigating buried polymer interfaces using sum frequency generation vibrational spectroscopy. *Prog. Polym. Sci.* **35**, 1376–1402 (2010).
21. E. A. Vogler, Protein adsorption in three dimensions. *Biomaterials* **33**, 1201–1237 (2012).
22. M. Chen, W. H. Briscoe, S. P. Armes, J. Klein, Lubrication at physiological pressures by polyzwitterionic brushes. *Science* **323**, 1698–1701 (2009).
23. Q. Shao, S. Jiang, Molecular understanding and design of zwitterionic materials. *Adv. Mater.* **27**, 15–26 (2015).
24. P. Jungwirth, B. Winter, Ions at aqueous interfaces: From water surface to hydrated proteins. *Annu. Rev. Phys. Chem.* **59**, 343–366 (2008).
25. W. H. Robertson, E. G. Diken, E. A. Price, J.-W. Shin, M. A. Johnson, Spectroscopic determination of the OH solvation shell in the $OH\cdot(H_2O)_n$ clusters. *Science* **299**, 1367–1372 (2003).

26. A. J. Hopkins, S. Schrödle, G. L. Richmond, Specific ion effects of salt solutions at the CaF_2/water interface. *Langmuir* **26**, 10784–10790 (2010).
27. T. L. Sun, T. Kurokawa, S. Kuroda, A. Bin Ihsan, T. Akasaki, K. Sato, M. A. Haque, T. Nakajima, J. P. Gong, Physical hydrogels composed of polyampholytes demonstrate high toughness and viscoelasticity. *Nat. Mater.* **12**, 932–937 (2013).
28. G. Petzold, S. Schwarz, Polyelectrolyte complexes in flocculation applications. *Adv. Polym. Sci.* **256**, 25–66 (2014).
29. B. L. Rivas, E. D. Pereira, M. Palencia, J. Sánchez, Water-soluble functional polymers in conjunction with membranes to remove pollutant ions from aqueous solutions. *Prog. Polym. Sci.* **36**, 294–322 (2011).
30. S. Y. Zhang, A. M. Bellinger, D. L. Glettig, R. Barman, Y.-A. L. Lee, J. Zhu, C. Cleveland, V. A. Montgomery, L. Gu, L. D. Nash, D. J. Maitland, R. Langer, G. Traverso, A pH-responsive supramolecular polymer gel as an enteric elastomer for use in gastric devices. *Nat. Mater.* **14**, 1065–1071 (2015).
31. S. Edmondson, V. L. Osborne, W. T. S. Huck, Polymer brushes *via* surface-initiated polymerizations. *Chem. Soc. Rev.* **33**, 14–22 (2004).
32. A. Salis, B. W. Ninham, Models and mechanisms of Hofmeister effects in electrolyte solutions, and colloid and protein systems revisited, *Chem. Soc. Rev.* **43**, 7358–7377 (2014).
33. M. Rodahl, F. Höök, A. Krozer, P. Brzezinski, B. Kasemo, Quartz crystal microbalance setup for frequency and *Q*-factor measurements in gaseous and liquid environments. *Rev. Sci. Instrum.* **66**, 3924–3930 (1995).
34. H. G. Tompkins, E. A. Irene, *Handbook of Ellipsometry* (William Andrew Publishing, Norwich, 2005).
35. M. Kobayashi, M. Terada, Y. Terayama, M. Kikuchi, A. Takahara, Direct synthesis of well-defined poly[{2-(methacryloyloxy)ethyl}trimethylammonium chloride] brush via surface-initiated atom transfer radical polymerization in fluoroalcohol. *Macromolecules* **43**, 8409–8415 (2010).
36. B. Li, B. Yu, W. T. S. Huck, W. Liu, F. Zhou, Electrochemically mediated atom transfer radical polymerization on nonconducting substrates: Controlled brush growth through catalyst diffusion. *J. Am. Chem. Soc.* **135**, 1708–1710 (2013).
37. J. J. I. Ramos, S. E. Moya, Water content of hydrated polymer brushes measured by an in situ combination of a quartz crystal microbalance with dissipation monitoring and spectroscopic ellipsometry. *Macromol. Rapid Commun.* **32**, 1972–1978 (2011).
38. D. Henry, The cataphoresis of suspended particles. Part I. The equation of cataphoresis. *Proc. R. Soc. London, Ser. A* **133**, 106–129 (1931).
39. C. Calero, J. Faraudo, D. Bastos-González, Interaction of monovalent ions with hydrophobic and hydrophilic colloids: Charge inversion and ionic specificity. *J. Am. Chem. Soc.* **133**, 15025–15035 (2011).
40. Q. Wei, M. Cai, F. Zhou, W. Liu, Dramatically tuning friction using responsive polyelectrolyte brushes. *Macromolecules* **46**, 9368–9379 (2013).
41. A. Wittemann, M. Ballauff, Interaction of proteins with linear polyelectrolytes and spherical polyelectrolyte brushes in aqueous solution. *Phys. Chem. Chem. Phys.* **8**, 5269–5275 (2006).
42. H. J. Bakker, J. L. Skinner, Vibrational spectroscopy as a probe of structure and dynamics in liquid water. *Chem. Rev.* **110**, 1498–1517 (2010).
43. I. V. Stiopkin, C. Weeraman, P. A. Pieniazek, F. Y. Shalhout, J. L. Skinner, A. V. Benderskii, Hydrogen bonding at the water surface revealed by isotopic dilution spectroscopy. *Nature* **474**, 192–195 (2011).
44. M. Sovago, R. K. Campen, G. W. H. Wurpel, M. Müller, H. J. Bakker, M. Bonn, Vibrational response of hydrogen-bonded interfacial water is dominated by intramolecular coupling. *Phys. Rev. Lett.* **100**, 173901 (2008).
45. J. Kim, G. Kim, P. S. Cremer, Investigations of polyelectrolyte adsorption at the solid/liquid interface by sum frequency spectroscopy: Evidence for long-range macromolecular alignment at highly charged quartz/water interfaces. *J. Am. Chem. Soc.* **124**, 8751–8756 (2002).
46. M. L. Berkowitz, D. L. Bostick, S. Pandit, Aqueous solutions next to phospholipid membrane surfaces: Insights from simulations. *Chem. Rev.* **106**, 1527–1539 (2006).
47. U. Raviv, J. Klein, Fluidity of bound hydration layers. *Science* **297**, 1540–1543 (2002).
48. Y. He, Q. Shao, S. Chen, S. Jiang, Water mobility: A bridge between the Hofmeister series of ions and the friction of zwitterionic surfaces in aqueous environments. *J. Phys. Chem. C* **115**, 15525–15531 (2011).
49. J.D. Willott, T. J. Murdoch, B. A. Humphreys, S. Edmondson, G. B. Webber, E. J. Wanless, Critical salt effects in the swelling behavior of a weak polybasic brush. *Langmuir* **30**, 1827–1836 (2014).
50. Y. Hou, G. M. Liu, Y. Wu, G. Zhang, Reentrant behavior of grafted poly(sodium styrenesulfonate) chains investigated with a quartz crystal microbalance. *Phys. Chem. Chem. Phys.* **13**, 2880–2886 (2011).

Acknowledgments: We thank C. Wu and Z. Hou for helpful discussions. We also thank Z. Liu and Z. He from the Institute of Chemistry, Chinese Academy of Sciences for help with adhesive force measurements. **Funding:** We acknowledge financial support from the National Program on Key Basic Research Project (2012CB933802), the National Natural Science Foundation of China (21374110, 21574121, 21234003, 91127042, 21273217, and 21421063), the Strategic Priority Research Program of the Chinese Academy of Sciences (XDB01020200), the Key Research Program of the Chinese Academy of Sciences, the Users with Excellence of the Hefei Science Center (2015HSC-UE008), the Fundamental Research Funds for the Central Universities (WK2340000066 and WK2340000064), and the Youth Innovation Promotion Association of the Chinese Academy of Sciences. **Author contributions:** G.L. and G.Z. designed the experiments. B.W., X.W., and Z.H. carried out the preparation of polyelectrolyte brushes and the combination of QCM-D and ellipsometry measurements. B.W., J.Y., Z.H., R.K., and J. Z. performed wettability, lubrication, adhesion, AFM, XPS, and protein adsorption experiments. K.T., J.Y., R.K., G.L., S.Y., and Y.L. collected and analyzed the SFG-VS data. G.L., G.Z., B.W., S.Y., Y.L., and V.S.J.C. interpreted the results and prepared the manuscript. All authors contributed to editing the manuscript. **Competing interests:** The authors declare that they have no competing interests. **Data and materials availability:** All data needed to evaluate the conclusions in the paper are present in the paper and/or the Supplementary Materials. Additional data related to this paper may be requested from the authors.

Submitted 18 March 2016
Accepted 11 July 2016
Published 5 August 2016
10.1126/sciadv.1600579

Citation: B. Wu, X. Wang, J. Yang, Z. Hua, K. Tian, R. Kou, J. Zhang, S. Ye, Y. Luo, V. S. J. Craig, G. Zhang, G. Liu, Reorganization of hydrogen bond network makes strong polyelectrolyte brushes pH-responsive. *Sci. Adv.* **2**, e1600579 (2016).